(Preprint) AAS 25-182

GOAL-ORIENTED TRAJECTORIES ABOUT MINOR BODIES USING SEQUENTIAL CONVEX PROGRAMMING: A STOCHASTIC APPROACH

Carmine Giordano[*], Stefano Campagnola[†], and Francesco Topputo[‡]

The exploration of minor bodies is crucial for understanding the solar system's origins and resource potential. Small satellites, appealing in this context, face challenges such as limited control, state uncertainties, and command errors. Traditional trajectory design methods, which focus on nominal paths, are labor-intensive and lack robustness. This work introduces a novel methodology combining polynomial chaos expansion and sequential convex programming to compute goal-oriented robust trajectories that account for uncertainties in dynamics, navigation, and control. Numerical simulations demonstrate the method effectiveness in providing robust, feasible solutions, emphasizing the need for a stochastic approach in uncertain environments.

INTRODUCTION

Recently, the exploration of minor bodies within the solar system has gained increasing interest due to their potential to reveal the origin of life,[1] explain the evolution of the solar system,[2] and provide resources for sustainable development of the humankind on Earth and in space.[3] On the other hand, small bodies also pose a substantial threat to life on Earth, as their impacts can cause catastrophic events.[4] For these reasons, the necessity of a thorough characterization of small bodies in terms of surface composition, internal structure, and physical features has become a primary objective in planetary science.[5] While ground-based surveys could be exploited to retrieve coarse estimates on the dimensions, shape, and rotational state, in-situ observations with robotic probes are required for detailed analyses and deeper evaluations of physical and dynamical properties.[6] In light of this, the scientific community has prioritized missions aimed at studying minor bodies.[7–11] Alongside large-scale missions, in recent times, there has been an increasing momentum in employing small platforms, such as CubeSats and SmallSats, in order to get considerable scientific return at significantly lower costs.[12,13] However, due to their limited size and mass constraints, miniaturized probes often rely on novel electric propulsion systems to maximize efficiency and minimize the propellant mass to be embarked.[14,15] Thus, small platforms are characterized by (1) limited–control authority (due to low thrust levels and a skeletal propellant budget), (2) large uncertainties in the state knowledge (due to novel techniques in navigation and/or limited access to on-ground facilities), (3) and large errors in command actuation (due to low-maturity components). These

[*]PostDoc Fellow, Department of Aerospace Science and Technology, Politecnico di Milano, via La Masa, 34, Milan, 20156, Italy.

[†]Mission Design Engineer, Outer Planet Mission Analysis Group, Jet Propulsion Laboratory, California Institute of Technology, Pasadena, California, 91109.

[‡]Full Professor, Department of Aerospace Science and Technology, Politecnico di Milano, via La Masa, 34, Milan, 20156, Italy.

characteristics, along with the inherent uncertainties typical of highly perturbed environments, necessitate the trajectory design to consider the full stochastic envelope of all possible trajectories in highly non-linear settings to avoid unflyable or unnecessarily expensive paths.
Traditionally, the conventional approach to design trajectories for close proximity operations (CPOs) about minor bodies focused only on computing the nominal path, that either was a long-term stable orbit, which could be challenging to find in extremely chaotic environments and have limited flexibility in terms of illumination and range, or designed by identifying scientifically valuable points and manually connecting them.[16–18] This last process is labor-intensive, time-consuming, and requires extensive human intervention. To address these challenges, in recent times, goal-oriented approaches have emerged, where high-level mission objectives are provided to an algorithm that autonomously computes the trajectory within a continuous replanning framework to best achieve the desired scientific objectives. This approach has been introduced by Surovik and Scheeres[19] by applying heuristic-guided reachability analyses in a receding horizon scheme with the aim to design trajectories with impulsive orbit control maneuvers that fulfill abstractly specified science goals.
Despite their potential, current goal-oriented approaches depend on reachability maps. While robust and suitable to be applied to onboard planning, reachability maps can be limiting, particularly for platforms equipped with continuous thrust systems. Additionally, even if they have been modified to consider also uncertainties in the dynamics, these approaches rely on a rather simplistic uncertainty quantification method, that could be unsuitable for highly perturbed settings and could misestimate the quantities of interest.
In this work, a novel methodology to compute *robust* goal-oriented trajectories about minor bodies is presented, embedding directly in the optimization problem the uncertainties in dynamics, navigation, and control. This approach transform the stochastic nonlinear optimal control problem, describing the uncertain goal-oriented trajectory design about minor bodies, in a deterministic convex programming problem by exploiting polynomial chaos expansion (PCE) and sequential convex programming (SCP)[20] with the aim to compute optimal trajectories that satisfy both engineering constraints and scientific goals in a stochastic sense.

PROBLEM INTRODUCTION

Given a spacecraft equipped with low thrust propulsion system flying close to a minor body, the robust goal-oriented minimum-fuel problem has the aim to find a trajectory satisfying all the scientific targets in a given timeframe in a stochastic sense while minimizing a stochastic metric for the use of the propellant. In this work, without loss of generality, the scientific goals will be represented as conical frusta[19,21] (Fig. 1). It is required that the spacecraft state distribution lies within the conical region with a certain probability, so that it is possible to observe relevant features a) within a given range, to respect a desired ground sampling distance and avoid safety concerns, b) and within a certain angle from the normal, to have a clear view of the feature, with reasonable certainty.

Thus, the stochastic goal-oriented minimum-fuel problem can be formalized as

Problem 1 (General stochastic goal-oriented minimum-fuel problem)**.**

$$\underset{\mathbf{u}(t)}{\text{Minimize}}\, J := -E\left[m(t_f)\right] \tag{1}$$

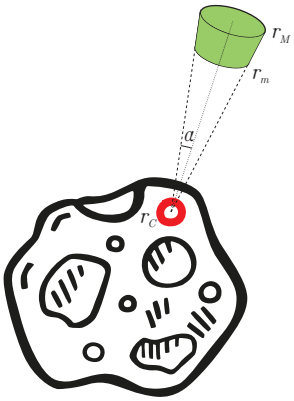

Figure 1: Representation of scientific goal. The green volume is the target region.

subject to

$$\begin{cases} \mathrm{d}\mathbf{r}_t = \mathbf{v}_t \, \mathrm{d}t \\ \mathrm{d}\mathbf{v}_t = \left(\mathbf{f}_f(\mathbf{x}_t, t) + \frac{\mathbf{T}_t}{m_t} \right) \mathrm{d}t + \boldsymbol{\omega}_t \, \mathrm{d}t \\ \mathrm{d}m_t = -\frac{\|\mathbf{T}_t\|}{I_{sp} g_0} \, \mathrm{d}t \\ \mathrm{d}\boldsymbol{\omega}_t = -\beta \boldsymbol{\omega}_t \, \mathrm{d}t + \Sigma \, \mathrm{d}W_t \end{cases} , \qquad \mathbf{x}(t_0) \sim \mathcal{N}(\mathbf{x}_0, \Sigma_0) \tag{2}$$

and

$$0 \leq \|\mathbf{T}_t\| \leq T_{\max} \tag{3}$$

and N_g scientific constraints

$$\mathbb{P}\mathrm{r}\left[\begin{cases} r_m \leq \|\mathbf{r}(t_i) - \mathbf{r}_{c_i}(t_i)\| \leq r_M & \text{(4a)} \\ \dfrac{\mathbf{r}(t_i) \cdot \mathbf{r}_{c_i}(t_i)}{\|\mathbf{r}(t_i)\| \|\mathbf{r}_{c_i}(t_i)\|} \leq \cos\alpha & \text{(4b)} \end{cases} \right] \geq \mathbb{P}\mathrm{r}_\delta \qquad \text{for some } t_i \in [t_0, t_f], \text{ for } i = 1, \ldots, N_g$$

Eq. (2) represents the stochastic dynamics as a system of stochastic differential equations in the Itô form, where $\mathbf{x} = [\mathbf{r}, \mathbf{v}, m]^T$ is the state, embedding the position, the velocity, and the mass, respectively, and $\boldsymbol{\omega}$ is a generic Gauss–Markov (GM) process, used to represent uncertainties in the dynamics, with $\beta = 1/\tau$ the autocorrelation factor, Σ denoting a generic diffusion term and W_t a Wiener process. $\mathbf{T}$ is the thrust vector and $T_{\max}$ its attainable maximum value, I_{sp} the thruster specific impulse, and g_0 gravitational acceleration at sea level.
The i-th scientific target is described as a chance constraint, with r_{c_i} the position of the feature, r_m and r_M, the minimum and maximum distance from the feature, respectively, and α the semi-aperture of the conical frustum, which requires that the probability to be in frustum is higher than a desired value $\mathbb{P}\mathrm{r}_\delta$.

PROBLEM IMPLEMENTATION

Gauss–Markov processes evalaution

Since that in Eqs. (2) the Gauss–Markov processes are decoupled from the state, they can be solved a-priori and used later on as time-dependent forcing terms. In this way, the original SDEs are transformed into simpler random ordinary differential equations (RODE).

Given a generic Gauss–Markov process (i.e., a stationary Ornstein–Uhlenbeck process), obeying the Langevin equation[22]

$$\mathrm{d}\omega_t = -\beta\omega_t \mathrm{d}t + \sigma \mathrm{d}W_t \tag{5}$$

it has solution equal to

$$\omega(t) = \omega_0 e^{-\beta(t-t_0)} + \int_{t_0}^{t_f} e^{-\beta(t-\tau)}\sigma W(t)\,\mathrm{d}\tau \tag{6}$$

A direct unique solution cannot be evaluated except in a statistical sense since the integral depends on the noise. One possible solution to this problem is to substitute the driving continuous noise, with a driving random sequence, that is a piecewise constant function $W(t) = W_k$ if $t \in [t_k, t_{k+1}]$. However, usually it requires a high number of terms to be accurate enough. An alternative approach is to use the Karhunen–Loève expansion. In this case, the process is approximated by a finite sum[23]

$$\omega(t) \simeq \sigma \sum_{i=1}^{d} \sqrt{\lambda_i} e_i(t) W_i \tag{7}$$

where $e_i(t)$ are eigenfunctions of the space spanned by the process covariance function, λ_i the associated eigenvalues, and W_i normal Gaussian random values. For normalized stationary Ornstein–Uhlenbeck processes, the eigenvalues are[23]

$$\lambda_i = \frac{1}{\omega_i^2 + \beta^2} \tag{8}$$

where ω_i are the ascending-ordered roots of the equation

$$\omega\cos(\omega T) + \left(-\frac{1}{2\beta} + \frac{\beta}{2}\right)\sin(\omega T) = 0 \tag{9}$$

The eigenfunctions are, instead, defined as[23]

$$e_i(t) = C_i\left(\omega_i \cos(\omega_i t) + \beta \sin(\omega_i t)\right) \tag{10}$$

with

$$C_i = \frac{1}{\sqrt{K_i}} \tag{11}$$

and

$$K_i = \frac{\beta}{2}\left(1 - \cos\left(2\omega_i T\right)\right) + \frac{\omega_i^2}{2}\left(T + \frac{\sin(2\omega_i T)}{2\omega_i}\right) + \frac{\beta^2}{2}\left(T - \frac{\sin(2\omega_i T)}{2\omega_i}\right) \tag{12}$$

Control parametrization

In order to facilitate the problem solution in a SCP setting, the coupling between state and control in Eqs. (2) could be eliminated by defining two new control variables, and a different metric for the mass[24]

$$\Gamma(t) = \frac{\|\mathbf{T}(t)\|}{m(t)}, \quad \boldsymbol{\tau}(t) = \frac{\mathbf{T}(t)}{m(t)}, \quad z(t) = \ln(m(t))$$

Additionally, in order to proper model uncertainties on the continuous thrust, the thrust acceleration variable is modeled as a GM process, that is

$$\mathrm{d}\boldsymbol{\tau}_t = -\beta\boldsymbol{\tau}_t\,\mathrm{d}t + \Sigma^{(\tau)}\,\mathrm{d}W_t \tag{13}$$

in which the variable $\Sigma^{(\tau)}$ is its standard deviation.
Its standard deviation can be retrieved by assuming that the engine can be modeled by exploiting a Gates-like model[25] for continuous thrust, that considers a proportional error $\delta\Gamma$ on the thrust magnitude, and additive errors $\delta\alpha$ and $\delta\beta$ on the azimuth and elevation angles, respectively, i.e.,

$$\boldsymbol{\tau} = (1+\delta\Gamma)\Gamma \begin{bmatrix} \cos(\alpha+\delta\alpha)\cos(\beta+\delta\beta) \\ \sin(\alpha+\delta\alpha)\cos(\beta+\delta\beta) \\ \sin(\beta+\delta\beta) \end{bmatrix} \tag{14}$$

By expanding the Eq. (14) and discarding higher-order terms, it can be found that the control can be modeled as a Gaussian variable with mean equal to $\boldsymbol{\tau}$ and standard deviation

$$\Sigma^{(\tau)} = \begin{bmatrix} \tau_x & -\tau_y & -\frac{\tau_x\tau_z}{\sqrt{\tau_x^2+\tau_y^2}} \\ \tau_y & \tau_x & -\frac{\tau_y\tau_z}{\sqrt{\tau_x^2+\tau_y^2}} \\ \tau_z & 0 & \sqrt{\tau_x^2+\tau_y^2} \end{bmatrix} \tag{15}$$

Thus, the noisy thrust acceleration $\tilde{\boldsymbol{\tau}}$ can be stated as

$$\tilde{\boldsymbol{\tau}} = \boldsymbol{\tau} + \Sigma^{(\tau)}\sigma \sum_{i=1}^{d} \sqrt{\lambda_i} e_i(t) W_i \tag{16}$$

Furthermore, in order to keep the equation of motion affine in the control, 3 new control variables are introduced

$$\tau_{xy} = \sqrt{\tau_x^2+\tau_y^2}, \qquad \tau_{xz} = -\frac{\tau_x\tau_z}{\tau_{xy}}, \qquad \tau_{yz} = -\frac{\tau_y\tau_z}{\tau_{xy}}$$

Chance constraints formulation

Uncertainties in the dynamics and control prevents any possible assumption on the evolution in time of the stochastic characteristics of the state. Hence, it is not possible to infer the distribution of the state at any time, different from the prescribed initial value. For this reason, the chance constraints defined in Eq. (4) are encoded as distributionally robust chance constraints (DRCC),[26] i.e., considering using a conservative formulation able to handle any arbitrary distribution of the state vector. However, DRCC can be formulated only for linear and purely quadratic constraints. Thus, the cone is Fig. 1 is approximated as the intersection of four planes, so that second order cone constraint in Eq. (4b) can be replaced by 4 linear constraints, that is

$$\mathbb{P}\mathrm{r}\left[HR\left(\mathbf{r}(t_i) - \mathbf{r}_{c_i}\right) \leq 0\right] \geq \mathbb{P}\mathrm{r}_\delta, \qquad \text{for some } t_i \in [t_0, t_f] \tag{17}$$

where H is a 4×3 matrix containing the normal of the planes

$$H = \begin{bmatrix} \cos(\alpha) & 0 & -\sin(\alpha) \\ 0 & \cos(\alpha) & -\sin(\alpha) \\ -\cos(\alpha) & 0 & -\sin(\alpha) \\ 0 & -\cos(\alpha) & -\sin(\alpha) \end{bmatrix} \tag{18}$$

Exploiting the DRCC formulation, Eq. (17) is reduced to

$$HR\left(\mu_r(t_i) - \mathbf{r}_{c_i}\right) + \sqrt{\frac{1-\varepsilon}{\varepsilon}}\sqrt{HR\Sigma_r R^T H^T} \tag{19}$$

with μ_r and Σ_r the mean and covariance matrix of the position.

Uncertainty quantification

Linear uncertainty quantification techniques may fail in proximity of minor bodies due to the chaotic and strongly perturbed environment. For this reason, a nonlinear method is required.[27] In this work, polynomial chaos expansion will be exploited, since it has been proven to accurately quantify the uncertainties in CPOs and it has been already effectively used within optimal control problems.[26,28] In PCE, the quantities under investigation, i.e., the state, are approximated using[29]

$$\hat{\mathbf{x}}(t, \boldsymbol{\xi}) = \sum_{\boldsymbol{\alpha} \in \Lambda_{p,d}} \mathbf{c}_{\boldsymbol{\alpha}}(t) \psi_{\boldsymbol{\alpha}}(\boldsymbol{\xi}) \tag{20}$$

where $\Lambda_{p,d}$ is a set of the multi-index of size d and order p defined on nonnegative integers, and $\boldsymbol{\xi} = [\xi_1, \ldots, \xi_d]$ is the set of input random variables.
Generation of a PCE means computing the generalized Fourier coefficients $\mathbf{c}_{\boldsymbol{\alpha}}(t)$. In this work, an intrusive approach will be exploited to this aim.
The intrusive approach solves for $\mathbf{c}_{\boldsymbol{\alpha}}(t)$ by performing a Galerkin projection of the governing stochastic equations onto the $\{\psi_{\boldsymbol{\alpha}}(\boldsymbol{\xi})\}$ subspace. By doing so, a number of ODE is added to the original problem to compute the PCE coefficient, and they are

$$\frac{\mathrm{d}\mathbf{c}_{\boldsymbol{\alpha}}(t)}{\mathrm{d}t} = \frac{1}{\langle \psi_{\boldsymbol{\alpha}}(\boldsymbol{\xi}), \psi_{\boldsymbol{\alpha}}(\boldsymbol{\xi}) \rangle} \left\langle \mathbf{f} \left(\sum_{\boldsymbol{\alpha} \in \Lambda_{p,d}} \mathbf{c}_{\boldsymbol{\alpha}}(t) \psi_{\boldsymbol{\alpha}}(\boldsymbol{\xi}),\ t \right), \psi_{\boldsymbol{\alpha}}(\boldsymbol{\xi}) \right\rangle \tag{21}$$

Assuming to use a normalized basis, Eq. (21) becomes

$$\dot{\mathbf{c}}_{\boldsymbol{\alpha}} = \mathit{F}(\mathbf{x}(t), \mathbf{u}(t), t) = \int_{\Gamma^d} \mathbf{f} \left(\sum_{\boldsymbol{\alpha} \in \Lambda_{p,d}} \mathbf{c}_{\boldsymbol{\alpha}}(t) \psi_{\boldsymbol{\alpha}}(\boldsymbol{\xi}),\ t \right) \psi_{\boldsymbol{\alpha}}(\boldsymbol{\xi}) \rho(\boldsymbol{\xi}) \mathrm{d}\boldsymbol{\xi} \tag{22}$$

The dynamics can be subdivided based on the dependence on the state and control

$$\mathbf{f}(\mathbf{x}(t), \mathbf{u}(t), t) = \mathbf{f}_f(\mathbf{x}, t) + B(\omega, t)\mathbf{u}(t) + \boldsymbol{C}(\omega, t) \tag{23}$$

Hence, Eq. (22) becomes

$$\dot{\mathbf{c}}_{\boldsymbol{\alpha}} = \int_{\Gamma^d} \mathbf{f}_f \left(\sum_{\boldsymbol{\alpha} \in \Lambda_{p,d}} \mathbf{c}_{\boldsymbol{\alpha}}(t) \psi_{\boldsymbol{\alpha}}(\boldsymbol{\xi}),\ t \right) \psi_{\boldsymbol{\alpha}}(\boldsymbol{\xi}) \rho(\boldsymbol{\xi}) \mathrm{d}\boldsymbol{\xi} + \hat{B}(t)\mathbf{u}(t) + \hat{\boldsymbol{C}}(t) \tag{24}$$

where the independence of the control and the Gauss–Markov processes from the state has been exploited together with the orthogonal properties associated to the PCE basis.
Solving the integral in Eq. (24) could be cumbersome and computational intensive. However, the use of sparse stochastic quadrature techniques can be helpful

$$\int_{\Gamma^d} \mathbf{f}_f \left(\sum_{\boldsymbol{\alpha} \in \Lambda_{p,d}} \mathbf{c}_{\boldsymbol{\alpha}}(t) \psi_{\boldsymbol{\alpha}}(\boldsymbol{\xi}),\ t \right) \psi_{\boldsymbol{\alpha}}(\boldsymbol{\xi}) \rho(\boldsymbol{\xi}) \mathrm{d}\boldsymbol{\xi} = \sum_{i=1}^{M} \mathbf{f}_f \left(\sum_{\boldsymbol{\alpha} \in \Lambda_{p,d}} \mathbf{c}_{\boldsymbol{\alpha}} \psi_{\boldsymbol{\alpha}}(\boldsymbol{\xi}_i) \right) \psi_{\boldsymbol{\alpha}}(\boldsymbol{\xi}_i) \omega_i \tag{25}$$

Substituting the integral with a sum is able to reduce the infinite multidimensional space in a manageable finite domain.

TRACKING CONTROL USING LINEAR QUADRATIC REGULATOR

The stochastic problem presented up to now it an open-loop problem. However, in this case, the trajectories dispersion tends to increase indefinitely, making possible to study only short portions of the trajectory. In a real-life scenario, trajectory correction maneuvers (TCMs) are inserted at certain prescribed times to control dispersion evolution. Usually, TCMs are computed by means of a predefined control policy. A linear feedback control, i.e.,

$$\hat{\boldsymbol{\tau}}_k = \tilde{\boldsymbol{\tau}}_k + \Pi_k \left(\hat{\mathbf{x}}_k - \mathbf{x}_k \right) \tag{26}$$

is usually used for its simplicity and efficiency. In this work, exploiting the PCE approximation of the state and the control structure given by Eq. (16), the feedback control can be rewritten as

$$\hat{\boldsymbol{\tau}}_k = \Pi_k \left(\sum_{\boldsymbol{\alpha} \in \Lambda_{p,d}} \mathbf{c}_{\boldsymbol{\alpha},k} \psi_{\boldsymbol{\alpha}}(\boldsymbol{\xi}) - \mathbf{c}_{\mathbf{0},k} \right) + \boldsymbol{\tau} + \Sigma^{(\tau)} \sigma \sum_{i=1}^{d} \sqrt{\lambda_i} e_i(t) W_i \tag{27}$$

Following this formulation, the dynamical equations in Eq. (24) are modified to include the feedback control. Specifically, the first term in Eq. (27) is included in $\mathbf{f}_f$, since it contains terms dependent only on $\mathbf{c}_{\boldsymbol{\alpha}}$ and $\psi_{\boldsymbol{\alpha}}$, the second term is (already) included in $\hat{B}$, while the last term is (already) embedded in $\hat{C}$.

The different linear feedback control policies depends on how the gain matrix Π_k is computed. While it can be appended in the decision variable vector, and found within the optimization problem, in this work, the linear quadratic regulator (LQR) is exploited to estimate the gain matrix with minimal additional computational effort. Since the control must both minimize the final mass and respect the chance constraints, the cost function of the LQR is chosen to be

$$J = -c_{0,m}^2 + \sum_{i=1}^{n} (\hat{\mathbf{x}}_i - \mathbf{x}_i)^T (\hat{\mathbf{x}}_i - \mathbf{x}_i)$$

where the sum on i counts for the target states.

Since the system considered in the SCP problem is designed to be finite-horizon and discrete-time, the gain matrix can be computed as[30]

$$\Pi_k = - \left(B_k^T F_{k+1} B_k \right)^{-1} \left(B_k F_{k+1} A_k \right) \tag{28}$$

where the matrix F_k is found iteratively backwards in time by the dynamic Riccati equation

$$F_{k-1} = A_k F_k A_k - \left(A_k^T F_k B_k \right) \left(B_k^T F_k B_k \right)^{-1} \left(B_k^T F_k A_k \right) + I \tag{29}$$

from the terminal condition $F_N = [0, 0, 0, 0, 0, 0, -1]^T$.

THE STOCHASTIC CONVEX MODEL

All the building blocks are then put together, and the problem is convexified following the paradigm of the SCP,[20] then discretized by subdividing the timespan $[t_0, t_f]$ into N segments. Scientific targets can be encoded by using the Big M method. Hence, Problem 1, a stochastic nonlinear optimal control problem, is converted in the following deterministic mixed-integer second-order cone constraint problem (MISOCP).

Problem 2 (Convex programming problem for the robust goal-oriented minimum-fuel problem)**.** Find $y = [\mathbf{c}_{\boldsymbol{\alpha},k}, \mathbf{u}_k, \boldsymbol{\nu}_k, \boldsymbol{\eta}_k],\ k = 1, \ldots, N$, such that

$$J := -c_{(z,\mathbf{0}),N} + \sum_{i=0}^{N} \lambda \|\boldsymbol{\nu}_k\|_1 + \sum_{i=0}^{N} \lambda \max(0, \eta_k) - \lambda_g \sum_{i=1}^{N_g} \min\left(1, \sum_{k=0}^{N} \gamma_{i,k}\right) \tag{30}$$

is minimized, subject to

$$\boldsymbol{\Delta} = \hat{A}\mathbf{c}_{\boldsymbol{\alpha}} + \hat{B}\mathbf{u} + \mathbf{q} + \hat{N}\boldsymbol{\nu} = \mathbf{0} \tag{31}$$

the control constraints

$$0 \leq \Gamma_k \leq T_{\max} e^{-\bar{z}_k} (1 - z_k + \bar{z}_k) + \eta_{1,k} \tag{32}$$

$$\|\boldsymbol{\tau}_k\| \leq \Gamma_k \tag{33}$$

$$\begin{cases} \sqrt{\tau_{x,k}^2 + \tau_{y,k}^2} \leq \tau_{xy,k} \\ \tau_{x,k}\tau_{z,k} + \tau_{xz,k}\tau_{xy,k} = 0 \\ \tau_{y,k}\tau_{z,k} + \tau_{yz,k}\tau_{xy,k} = 0 \end{cases} \tag{34}$$

and the goal constraints

$$HR(\mathbf{c}_{\mathbf{r},\mathbf{0}}(t_i) - \mathbf{r}_{c_i}) + \sqrt{\frac{1-\varepsilon}{\varepsilon}} \|HR\mathbf{c}_{\mathbf{r},\boldsymbol{\alpha}}(t_i)\| \leq M(1 - \gamma_{i,k}) \tag{35}$$

and the trust region constraint

$$\|\mathbf{c}_{\boldsymbol{\alpha}} - \bar{\mathbf{c}}_{\boldsymbol{\alpha}}\|_1 + q\|\mathbf{u} - \bar{\mathbf{u}}\|_1 \leq R \tag{36}$$

The variable $\gamma_{i,k}$ is the index binary variable for the single scientific target, i.e., it is 1 if the target i is respected at point k, and 0 otherwise, with M a sufficiently large value. Last term in Eq. (30) is a reward function, that is 0 whenever the goal is not reached and it decreases with the number of nodes satisfying the goal, being $-\lambda_g$ when all the targets are satisfied at least once.

NUMERICAL SIMULATIONS

The performances of the SCP algorithm to solve the robust goal-oriented problem about a minor body are evaluated by means of several numerical simulations. In SCP, the basic algorithm foresees to solve the convex programming problem recursively. However, MISOCPs are usually more difficult to solve than simple SOCPs. For this reason, it is preferable to reduce the times the MISOCP is solved. The MISOCP is solved iteratively until the nonlinear constraint metric $\|\mathbf{h}\|_\infty$ is below a certain threshold $\bar{h}$. When this condition is satisfied, the binary variable γ is fixed and so a simple SOCP is solved in the following iterations.

Iterations are stopped successfully if the maximum nonlinear constraint violation and the improvement of the modified mass metric are below a certain threshold, i.e, $\|\mathbf{h}\|_1 \leq \varepsilon_h$ and $\bar{z} - z \leq \varepsilon_z$. On the other hand, the procedure is terminated without success if the relative difference of the solution vector in two consecutive iterations is below a certain threshold (i.e., $\|\bar{x} - x\|_1 \leq \varepsilon_x$), meaning that there is not any improvement in the solution, or if the trust region radius is too small (i.e., $R \leq \varepsilon_R$). All these relevant parameter are provided in Table 1.

Table 1: SCP parameters

Parameter	Value
λ	100.0
M	100.0
R_0	1000.0
q	100.0
$(\varepsilon_h, \varepsilon_z, \varepsilon_x, \varepsilon_R)$	$\left(10^{-6}, 10^{-4}, 10^{-8}, 10^{-4}\right)$

Simulations overview

In order to test the algorithm presented, a CubeSat flying about a small asteroid in a Sun-stabilized terminator orbit (SSTO) is used as test case scenario. The scenario is based on the ESA's mission SATIS.[31] SATIS is a 12XL CubeSat having the aim to reach the asteroid Apophis before its flyby with the Earth in 2029 and perform scientific activities to characterize the asteroid before and after its close encounter. In this case, the target is modeled as a tri-axial ellipsoid.[32] The CubeSat is considered to be placed on an SSTO, generated with the procedure in Takahashi and Scheeres,[33] and perturbed by the SRP and the gravitational perturbatons by the Sun, the Earth, and the Moon. This choice is common in CPOs close to minor bodies due to the stability of this kind of orbit in a high-perturbed environment, like the one of Apophis close to its close encounter. A single TCM at $3.5\,\mathrm{d}$ is considered.
Table 2 summarizes the main values of both target and spacecraft associated to the test case scenario.

Table 2: Test case scenario parameters. $\mathcal{U}$ indicates the uniform distribution.

	Parameter	Value	
Spacecraft	Initial orbit semimajor axis a_0	$\mathcal{U}(0.6\,\mathrm{km}, 1.5\,\mathrm{km})$	
	m_0	$25\,\mathrm{kg}$	
	$T_{\max}$	$2\,\mathrm{mN}$	
	I_{sp}	$1500\,\mathrm{s}$	
	C_r	1.3	
	A	$1.5\,\mathrm{m}^2$	
Main body	Gravity type	Tri-axial ellipsoid	
	μ	$2.736\,463 \times 10^{-9}\,\mathrm{km}^3/\mathrm{s}^2$	
	(a, b, c)	$(228.966\,\mathrm{m}, 159.026\,\mathrm{m}, 139.798\,\mathrm{m})$	[32]
	ω	$283.46\,^\circ/\mathrm{d}$	[34]
Goals	α	20°	
	r_m	$0.5\,\mathrm{km}$	
	r_M	$5\,\mathrm{km}$	
Uncertainties	σ_{r0}	$15\,\mathrm{m}$ (1% range)	Adapted from[35]
	σ_{v0}	$15\,\mathrm{mm/s}$ (1% velocity)	
	σ_Γ	1% magnitude	
	$\sigma_{(\alpha,\beta)}$	$1\,\mathrm{deg}$	
	β	$1/86400\,1/\mathrm{s}$	

The test case setting is made of 20 simulations with random initial conditions and random targets (distributed uniformly on the target surface), and with the characteristic provided in Table 3 are performed. All the simulations are carried out in Julia, on a 8-core Intel Core i7-10870H@2.20GHz computer with 32 GB of RAM.

Results

An example solution is provided in Fig. 2. This solution has been selected as example, since it shows clearly the impact of uncertainties in fulfilling scientific objectives. Indeed, it can be noted

Table 3: Simulation parameters

Parameter	Value
Time of Flight	7 d
Initial time t_0	January 1, 2029
Number of goals N_g	10
Maximum runtime	2700 s
Maximum iterations	50

that targets are respected only at the beginning and at the end of trajectory. This behavior, although not general, depends on the evolution of the dispersion, and how large dispersions prevent the targets to be satisfied. In fact, Fig. 3 shows the evolution of the dispersion over time. It can be noted that the targets are satisfied when the dispersion has lower values (i.e., at the beginning and towards the end). Additionally, the efficacy of the LQR to control the dispersion can be also observed.

Figures 4 shows the results of the numerical simulation. Two different discretization methods, a low-order Hermite Legendre–Gauss–Lobatto (LGL-3) collocation method and a First-Order Hold (FOH) control interpolation method are compared in terms of convergence ratio and computational times. The time metric is the 90-th percentile of the converged solutions. Results are similar to the one of the deterministic problem.[36] FOH is able to have better convergence properties even if longer computational times are required, while LGL-3 is faster but it exhibits lower convergence rates.

Comparison with deterministic solutions

Uncertainty in the dynamics and control can perturb significantly the real path of a spacecraft with respect to the nominal deterministic trajectory. These deviations can be so relevant that the real trajectory is not able to satisfy anymore the scientific goals, as intended. As a matter of fact, it could happen that Problem 2 can be unfeasible (and so it can not converge) if a deterministic solution in terms of targets to be satisfied is given as initial guess.
In order to quantify and assess this behavior, a test made of 50 different simulations, with random generated targets has been performed, solving three different problems:

1. the deterministic problem (solved as in[36]), indicated with D;
2. the stochastic problem, hot-started with the deterministic problem target matrix γ (i.e., without solving the mixed-integer problem), indicated with S*;
3. the stochastic problem from scratch (i.e., solving the mixed-integer problem to find γ), indicated with S.

The 50 simulations show different behaviors that can be grouped in four categories:

- **S=S*=D**. In 1 case (2% of the cases), the deterministic solution is optimal also from the stochastic point of view, meaning that D, S*, and S provide the same solutions in terms of target matrix and control profile.
- **S=S*≠D**. In 7 cases (14%), the target matrix is the same in both D and S, but the control profile is different. Of course, S* and S show the same control profile.
- **S≠S***. In 4 cases (8%), S* and S have different optimal target matrices, with S being cheaper, meaning that the deterministic target matrix is not optimal in the stochastic sense.

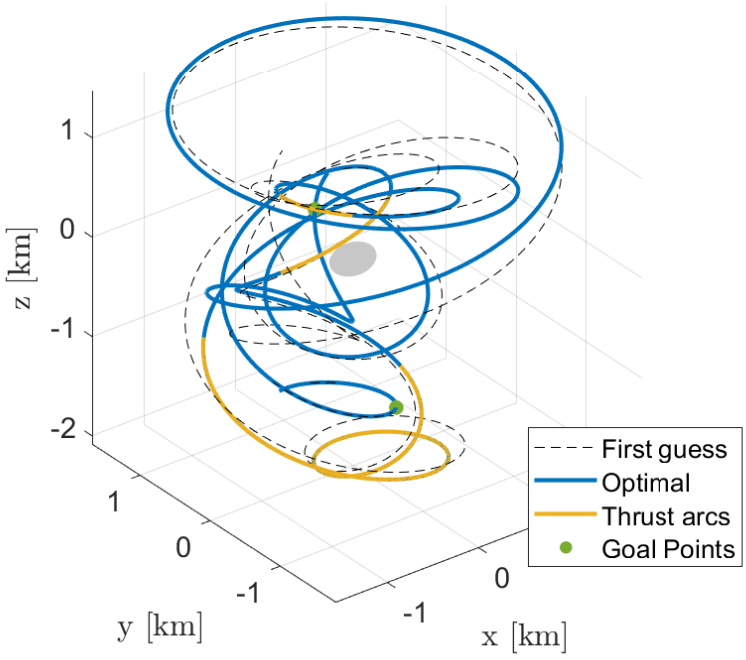

(a) Optimal trajectory.

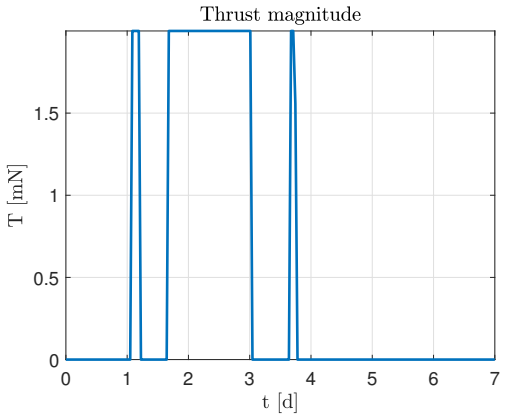

(b) Control profile.

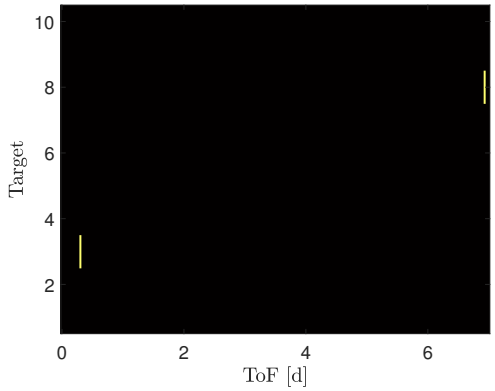

(c) Scientific constraints map. Yellow indicates when a target is respected.

Figure 2: Optimal solution example.

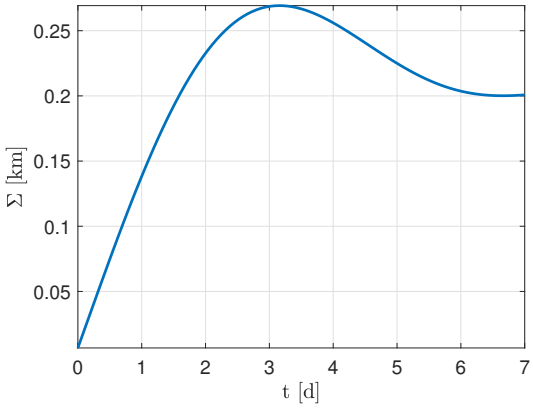

Figure 3: Evolution of the dispersion over time.

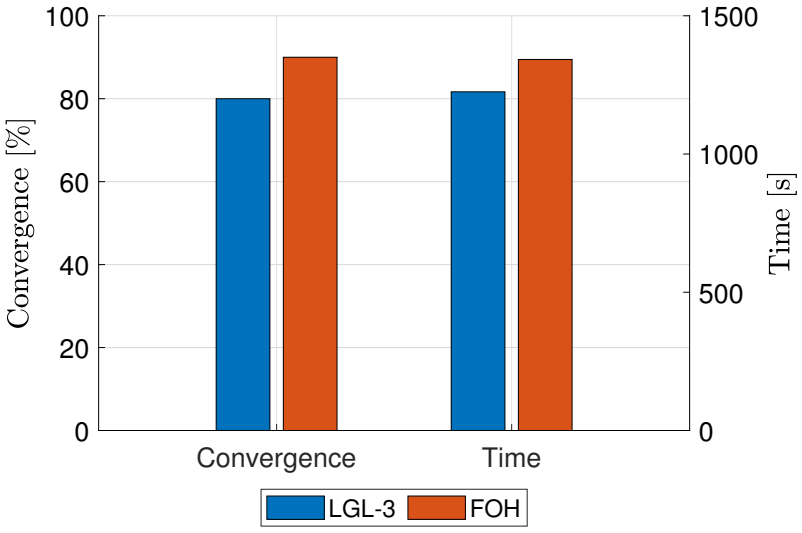

Figure 4: Test case scenario condensed results.

- **Infeasible S***. In 28 cases (76%), the problem S* is infeasible, meaning that the target matrix coming from D cannot give a feasible solution in stochastic sense.

The last three cases are the most interesting to be analyzed further.
Figure 5 shows an example for the case S=S*≠D. It can be noted that in the stochastic solution the thrust profile is slightly changed (Fig. 5a). This tweak in the control moves the optimal nominal state during the observation of target #10 closer to the cone axis (Fig. 5c). This allows the stochastic scientific target to be respected.
An example for cases with S≠S* is given in Figs. 6 and 7. In both cases, the number of targets observed is 2, but the total thrust time for the case S* is $1.75\,\mathrm{d}$, while it is only $1.575\,\mathrm{d}$ for S. Hence, while it is still possible to find a stochastic solution starting from the deterministic result, the full stochastic optimal trajectory allows to a 10% reduction in the propellant use.
In the last cases, S* does not converge due to infeasibility of at least one target chance constraint. On the other hand, an optimal stochastic solution can be found. It is the most frequent record, and an example is provided in Fig. 8. In the provided solution, only 3 targets are satisfied for problem S, in opposite to the 4 of problems D (and S*). This is mainly related to the fact that in the deterministic solution a long thrusting arc is needed to maximize the scientific output (Fig. 8a). As consequence, due to control errors, the dispersion grows significantly. Additionally, the LQR is not able to control it anymore. Conversely, the stochastic solution flies a lower dispersion trajectory and the state distribution is able to fit in all the target conical frusta. Indeed, in this case, the stochastic solution trades a lower number of target for a more robust trajectory.
It should be noted, however, that the example provided is peculiar. In most of the cases where S* is infeasible, the number of targets does not change, but it changes which target is satisfied and when during the trajectory. As a matter of fact, S* would require to satisfy the scientific constraints when the dispersion is too high and cannot be reduced, while the solution for the problem S finds the targets to be satisfied when the dispersion is lower (e.g., at the beginning or after the TCM).

CONCLUSION

In this work, an algorithm to compute robust goal-oriented fuel-optimal trajectories for low-thrust spacecraft about minor bodies is introduced. The methodology is based on a combination of sequential convex problem and polynomial chaos expansion. Under the SCP framework and exploiting the intrusive PCE formulation, the stochastic nonlinear problem is translated in a mixed-integer second-order cone constraint problem, that is solved iteratively to find the optimal trajectory. Numerical simulations are used to evaluate convergence and computational effort. Two different discretization methods have been tested and no significant difference has been found in test case scenario. The algorithm is able to provide optimal solutions in about 1200 seconds with a convergence rate of about the 80%. Additionally, a comparison with deterministic solution have proven that in this context the use of a robust stochastic approach is needed to avoid to fly unfeasible trajectories for the scientific point of view.

ACKNOWLEDGMENT

This project is part of CASTOR, a project that has received funding from the European Union's Horizon Europe research and innovation programme under the Marie Skłodowska-Curie grant agreement no. 101103826.
Part of this research was carried out at the Jet Propulsion Laboratory, California Institute of Technology, under a contract with the National Aeronautics and Space Administration (80NM0018D0004).

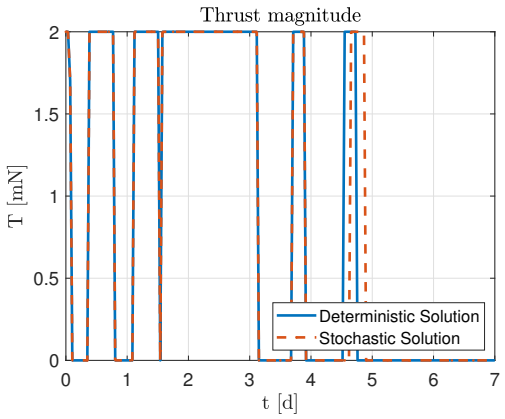

(a) Control profile.

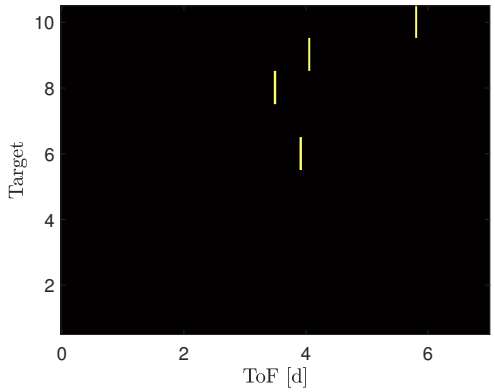

(b) Scientific constraints map. Yellow indicates when a target is respected.

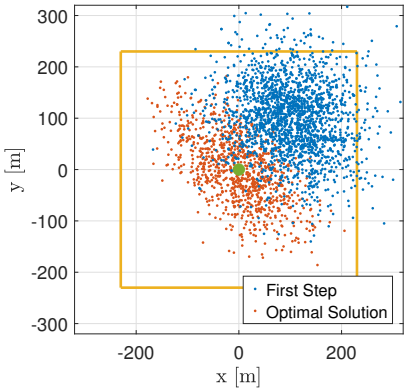

(c) Scatter plot of target #10. Green dot is the cone axis, yellow square is the projection of the four planes to be respected at the target nominal range from the asteroid.

Figure 5: Example for the case S=S*≠D.

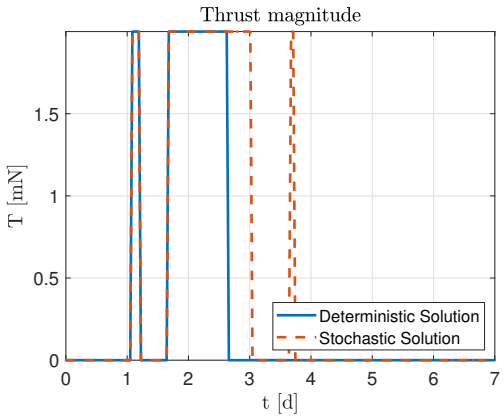

(a) Control profile.

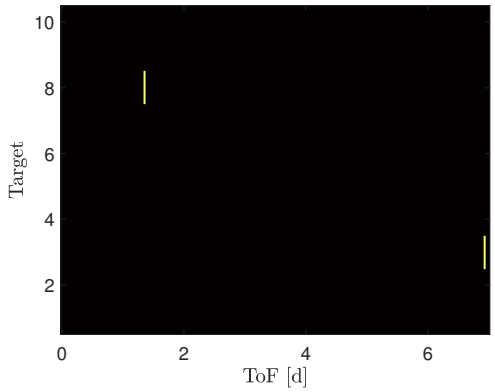

(b) Scientific constraints map. Yellow indicates when a target is respected.

Figure 6: Example for the case S≠S*: Solution of D and S*.

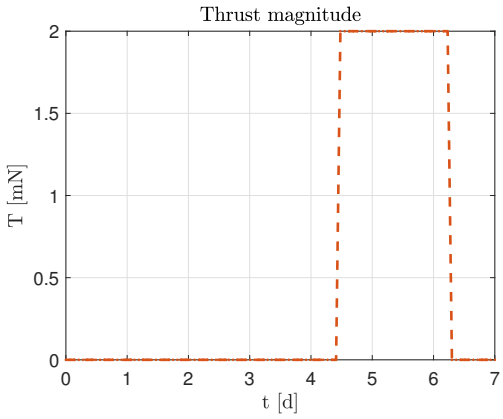

(a) Control profile.

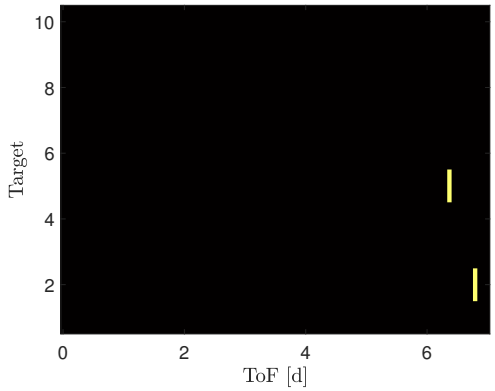

(b) Scientific constraints map. Yellow indicates when a target is respected.

Figure 7: Example for the case S≠S*: Solution of S.

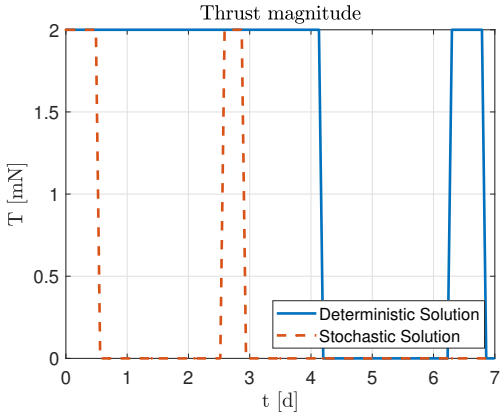

(a) Control profile for D and S. S* not reported due to infeasibility.

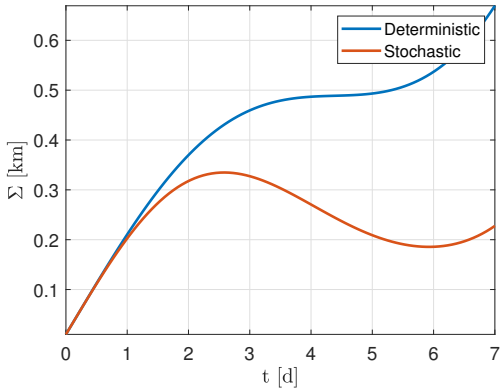

(b) Dispersion evolution for D and S. S* not reported due to infeasibility.

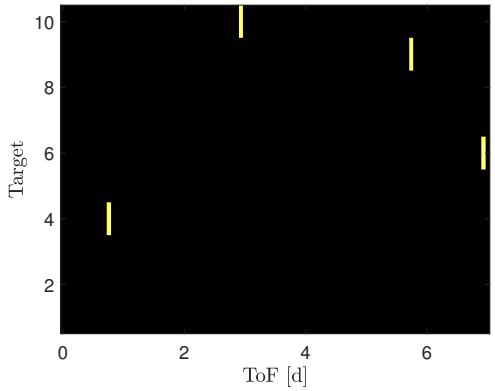

(c) Scientific constraints map for D and S*.

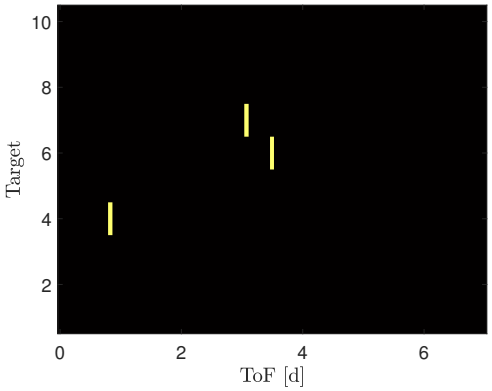

(d) Scientific constraints map for S.

Figure 8: Example for the case with infeasible S*.

REFERENCES

[1] J. Oro, T. Mills, and A. Lazcano, "Comets and life in the universe," *Advances in Space Research*, Vol. 15, No. 3, 1995, pp. 81–90.

[2] E. Asphaug, "Growth and evolution of asteroids," *Annual Review of Earth and Planetary Sciences*, Vol. 37, No. 1, 2009, pp. 413–448.

[3] A. Hein, M. Saidani, and H. Tollu, "Exploring Potential Environmental Benefits of Asteroid Mining," *69th International Astronautical Congress (IAC), Bremen, Germany, 1–5 October 2018*, 2018.

[4] C. R. Chapman, "The hazard of near-Earth asteroid impacts on earth," *Earth and Planetary Science Letters*, Vol. 222, No. 1, 2004, pp. 1–15.

[5] S. B. A. G. (SBAG), *Goals and Objectives for the Exploration and Investigation of the Solar System's Small Bodies*.

[6] J. C. Castillo-Rogez, M. Pavone, J. A. Hoffman, and I. A. Nesnas, "Expected science return of spatially-extended in-situ exploration at small solar system bodies," *2012 IEEE Aerospace Conference*, IEEE, 2012, pp. 1–15.

[7] D. Lauretta, S. Balram-Knutson, E. Beshore, W. Boynton, C. Drouet d'Aubigny, D. DellaGiustina, H. Enos, D. Golish, C. Hergenrother, E. Howell, *et al.*, "OSIRIS-REx: sample return from asteroid (101955) Bennu," *Space Science Reviews*, Vol. 212, 2017, pp. 925–984.

[8] K.-H. Glassmeier, H. Boehnhardt, D. Koschny, E. Kührt, and I. Richter, "The Rosetta mission: flying towards the origin of the solar system," *Space Science Reviews*, Vol. 128, 2007, pp. 1–21.

[9] P. Lord, S. Tilley, D. Y. Oh, D. Goebel, C. Polanskey, S. Snyder, G. Carr, S. M. Collins, G. Lantoine, D. Landau, *et al.*, "Psyche: Journey to a metal world," *2017 IEEE Aerospace Conference*, IEEE, 2017, pp. 1–11.

[10] M. Kueppers, P. Martino, I. Carnelli, and P. Michel, "Ramses–ESA's Study for a Small Mission to Apophis," *AAS/Division for Planetary Sciences Meeting Abstracts*, Vol. 55, 2023, pp. 201–08.

[11] N. L. Chabot, A. S. Rivkin, A. F. Cheng, O. S. Barnouin, E. G. Fahnestock, D. C. Richardson, A. M. Stickle, C. A. Thomas, C. M. Ernst, R. T. Daly, *et al.*, "Achievement of the planetary defense investigations of the Double Asteroid Redirection Test (DART) mission," *The Planetary Science Journal*, Vol. 5, No. 2, 2024, p. 49.

[12] A. Poghosyan and A. Golkar, "CubeSat evolution: Analyzing CubeSat capabilities for conducting science missions," *Progress in Aerospace Sciences*, Vol. 88, 2017, pp. 59–83, 10.1016/j.paerosci.2016.11.002.

[13] R. Walker, D. Binns, C. Bramanti, M. Casasco, P. Concari, D. Izzo, D. Feili, P. Fernandez, J. G. Fernandez, P. Hager, *et al.*, "Deep-space CubeSats: thinking inside the box," *Astronomy & Geophysics*, Vol. 59, No. 5, 2018, pp. 24–30, 10.1093/astrogeo/aty232.

[14] A. C. Morelli, A. Mannocchi, C. Giordano, F. Ferrari, and F. Topputo, "Initial Trajectory Assessment of a low-thrust option for the RAMSES Mission to (99942) Apophis," *Advances in Space Research*, Vol. 73, No. 8, 2024, pp. 4241–4253.

[15] F. Topputo, Y. Wang, C. Giordano, V. Franzese, H. Goldberg, F. Perez-Lissi, and R. Walker, "Envelop of reachable asteroids by M-ARGO CubeSat," *Advances in Space Research*, Vol. 67, No. 12, 2021, pp. 4193–4221.

[16] F. Ferrari, V. Franzese, M. Pugliatti, C. Giordano, and F. Topputo, "Trajectory options for hera's milani cubesat around (65803) didymos," *The Journal of the Astronautical Sciences*, Vol. 68, No. 4, 2021, pp. 973–994.

[17] A. Accomazzo, P. Ferri, S. Lodiot, J.-L. Pellon-Bailon, A. Hubault, R. Porta, J. Urbanek, R. Kay, M. Eiblmaier, and T. Francisco, "Rosetta operations at the comet," *Acta Astronautica*, Vol. 115, 2015, pp. 434–441.

[18] P. G. Antreasian, C. D. Adam, K. Berry, J. Geeraert, K. M. Getzandanner, D. Highsmith, J. M. Leonard, E. J. Lessac-Chenen, A. H. Levine, J. V. McAdams, *et al.*, "OSIRIS-REx Proximity Operations and Navigation Performance at Bennu," *AIAA SCITECH 2022 Forum*, 2022, p. 2470.

[19] D. A. Surovik and D. J. Scheeres, "Adaptive reachability analysis to achieve mission objectives in strongly non-keplerian systems," *Journal of Guidance, Control, and Dynamics*, Vol. 38, No. 3, 2015, pp. 468–477.

[20] D. Malyuta, T. P. Reynolds, M. Szmuk, T. Lew, R. Bonalli, M. Pavone, and B. Açıkmeşe, "Convex optimization for trajectory generation: A tutorial on generating dynamically feasible trajectories reliably and efficiently," *IEEE Control Systems Magazine*, Vol. 42, No. 5, 2022, pp. 40–113.

[21] A. Rizza, C. Giordano, and F. Topputo, "A goal-oriented guidance approach for binary asteroids exploration," *Astrodynamics*, 2024. In press.

[22] B. Schutz, B. Tapley, and G. H. Born, *Statistical orbit determination*. Elsevier, 2004.

[23] S. Corlay and G. Pages, "Functional quantization based stratified sampling methods, to appear in Monte Carlo Methods and Appl," *arXiv preprint arXiv:1008.4441*, 2014.

[24] Z. Wang and M. J. Grant, "Minimum-fuel low-thrust transfers for spacecraft: A convex approach," *IEEE Transactions on Aerospace and Electronic Systems*, Vol. 54, No. 5, 2018, pp. 2274–2290.

[25] K. Oguri and J. W. McMahon, "Robust spacecraft guidance around small bodies under uncertainty: Stochastic optimal control approach," *Journal of Guidance, Control, and Dynamics*, Vol. 44, No. 7, 2021, pp. 1295–1313.

[26] Y. K. Nakka, A. Liu, G. Shi, A. Anandkumar, Y. Yue, and S.-J. Chung, "Chance-constrained trajectory optimization for safe exploration and learning of nonlinear systems," *IEEE Robotics and Automation Letters*, Vol. 6, No. 2, 2020, pp. 389–396.

[27] N. Michelotti, A. Rizza, C. Giordano, and F. Topputo, "Comparison of uncertainty propagation techniques in small-body environment," *arXiv preprint arXiv:2408.05970*, 2024.

[28] C. Giordano and F. Topputo, "Analysis, Design, and Optimization of Robust Trajectories in Cislunar Environment for Limited-Capability Spacecraft," *The Journal of the Astronautical Sciences*, Vol. 70, No. 6, 2023, p. 53.

[29] B. A. Jones, A. Doostan, and G. H. Born, "Nonlinear propagation of orbit uncertainty using non-intrusive polynomial chaos," *Journal of Guidance, Control, and Dynamics*, Vol. 36, No. 2, 2013, pp. 430–444.

[30] G. Chow, *Analysis and Control of Dynamic Economic Systems*. R.E. Krieger, 1986.

[31] R. Walker, "Overview of ESA Lunar & Interplanetary CubeSat Missions," *Interplanetary Small Satellite Conference*, 2023.

[32] G. Valvano, O. C. Winter, R. Sfair, R. Machado Oliveira, G. Borderes-Motta, and T. Moura, "APOPHIS–effects of the 2029 Earth's encounter on the surface and nearby dynamics," *Monthly Notices of the Royal Astronomical Society*, Vol. 510, No. 1, 2022, pp. 95–109.

[33] S. Takahashi and D. J. Scheeres, "Higher-order corrections for frozen terminator orbit design," *Journal of Guidance, Control, and Dynamics*, Vol. 43, No. 9, 2020, pp. 1642–1655.

[34] P. Pravec, P. Scheirich, J. Ďurech, J. Pollock, P. Kušnirák, K. Hornoch, A. Galad, D. Vokrouhlickỳ, A. Harris, E. Jehin, *et al.*, "The tumbling spin state of (99942) Apophis," *Icarus*, Vol. 233, 2014, pp. 48–60.

[35] K. Berry, K. Getzandanner, M. C. Moreau, P. G. Antreasian, A. T. Polit, H. L. Enos, D. S. Lauretta, and M. Nolan, "Revisiting OSIRIS-REx touch-and-go (TAG) performance given the realities of asteroid Bennu," *Annual AAS Guidance, Navigation and Control Conference*, No. GSFC-E-DAA-TN77488, 2020.

[36] C. Giordano, S. Campagnola, and F. Topputo, "Goal-oriented trajectories about minor bodies using Sequential Convex Programming: A Deterministic Approach," *2025 AAS/AIAA Space Flight Mechanics Meeting*, 2025.